Identification of estrogen receptor α ligands with virtual screening techniques

Sanna P. Niinivehmas,[‡1] Elangovan Manivannan,[‡1,2] Sanna Rauhamäki,[1] Juhani Huuskonen[3] and Olli T. Pentikäinen*[1]

1 University of Jyvaskyla, Department of Biological and Environmental Science & Nanoscience Center, P.O. Box 35, FI-40014 University of Jyvaskyla, Finland

2 School of Pharmacy, Devi Ahilya University, Indore-452001, Madhya Pradesh, India

3 University of Jyvaskyla, Department of Chemistry & Nanoscience Center, P.O. Box 35, FI-40014 University of Jyvaskyla, Finland

*to whom correspondence should be addressed:

Phone: +358-40-5216913

E-mail: olli.t.pentikainen@jyu.fi

[‡]Authors contributed equally to this work

Abstract

Virtual screening (VS) is an attractive, cost-effective approach to identify novel bioactive small molecules. Unfortunately, there is no universal VS strategy that would guarantee high hit rates for the selected biological target, but each target requires distinct, fine-tuned solutions. Here, we have used a widely applied drug discovery target, estrogen receptor α (ERα), for the comparison of the effectiveness and usefulness of ligand-based method common pharmacophore hypothesis, and structure-based methods molecular docking and negative image-based screening as potential VS tools. Firstly, we identified an already known active ligand from the widely-used bechmarking decoy molecule set. Secondly, although VS against one commercially available database with approximately 100,000 drug-like molecules did not retrieve many testworthy hits, one novel hit molecule was identified. Thirdly, our small virtual compound collection with easy-to-synthesize molecules yielded some hit candidates, which were synthezised and found to be active as predicted.

Keywords

Estrogen receptor alpha; Virtual screening; Ligand discovery; Pharmacophore modeling; 3D-QSAR; Molecular docking; Negative image

Electronic supplementary material

The supporting information contains four additional figures (Fig. S1-S4), two additional tables (Table S1 and Table S2), and detailed synthesis and characterization data for molecules 1-5.

Introduction

In the modern drug discovery research, computational tools are increasingly used for cost-effective and rapid identification of new drug candidate molecules.[1] Especially, the development of virtual screening (VS) approaches gains attention because it offers an attractive approach to identify novel bioactive molecules from the chemical libraries.[1a] VS protocols can be designed to meet any specific requirement depending on the availability of the known ligands and/or target structure information.

VS methods can be classified under two main categories: ligand-based and protein structure-based VS.[2] Ligand-based VS is in practice the only solution when the structure of the target protein is absent, and cannot be reliably modeled. Ligand-based VS methods use the existing structure-activity data and calculated physicochemical properties of known bioactive molecules. Ligand-based VS includes methods such as three-dimensional (3D) quantitative structure-activity relationship (QSAR),[3] two-dimensional (2D) fingerprint similarity search,[4] and pharmacophore hypothesis.[5] In contrast, protein structure-based VS uses the 3D-structure information of a target molecule. From these methods molecular docking is the most commonly used.[6] However, molecular docking is computationally more expensive than ligand-based techniques, and the scoring functions associated with docking are not always effective in prioritizing the active molecules.[7] Although, all of the above mentioned VS methods have been proven to be useful in hit identification, each method also has their its pitfalls.[8] Accordingly, ligand- and protein structure-based VS have also been integrated, e.g. through docking based ligand alignment has been applied with 3D-QSAR methods.[9] Furthermore, in negative image-based (NIB) screening the ligand binding pocket (LBP) of the protein is described as a mimic of the ligand, which again, can be rapidly compared against library of small molecules with typical ligand-based methods. [10] Also the comparison of several methods can be a useful way to obtain more knowledge about the requirements for high affinity binding. [11]

Estrogen receptor (ER) is a nuclear hormone receptor, which functions as a mediator of estrogen's action in different parts of the body, and is an established target for drug development in infertility management, contraception, menopausal hormone replacement therapy, and endocrine based breast cancer therapy. [12] Among ERα binding ligands, selective ER modulators (SERMs) have received a remarkable impact in pharmaceutical

development for osteoporosis and estrogen sensitive cancer. Because of the availability of the X-ray crystal structure-ligand complexes and a large number of chemically diverse active ligands, ERα has been widely used in the development of VS methods,[13] and was thus chosen as the test system for comparative evaluation of both ligand- and structure-based VS methods.

In brief, the aim of this study was to compare the effectiveness of the ligand- and structure-based VS methods using ERα ligands belonging to distinct chemotypes, and their bio-molecular target ERα as a test system. Furthermore, we tested the developed models in the discovery of ERα ligands.

Experimental

Biochemical Data and Preparation of Datasets

In this study, we have used two data sets, referred as DS1 and DS2. DS1 contains carefully chosen 101 chemically diverse SERMs from ChEMBL database[14] with homogenous ERα inhibitory activity with pIC_{50}-values (i.e., $-\log(IC_{50})$) ranging from 5 to 9.7 (Supplementary Tables S1 and S2). DS1 ligands belong into 18 different chemotypes (Supplementary Table S1), from which the most active molecules have a benzoxathin or a 2-aryl benzothiophene scaffold. DS2 constitutes of a set of ERα antagonists (n = 39) and a large number of ER decoy molecules (n = 1395) provided within the Directory of Useful Decoys (DUD) [15]. To complement the comparability of DS1, the same DUD decoy molecules (n = 1395) were also added to it. The 3D structures of both DS1 and DS2 ligands were prepared using Ligprep 2.5 (Schrödinger Inc, New York, NY), where the stereochemistry of all the compounds was retained, while the protonation state for all the ionizable groups was set at pH 7.4. A conformational search was performed using ConfGen[16] with pre-minimization using MMFF94 force field[17] with distant dependent dielectric solvent model.

Common Pharmacophore Hypothesis Model Generation

The common pharmacophore hypothesis (CPH) based 3D-QSAR models were built within the PHASE v3.3[18]. For 3D-QSAR model development and validation purpose, DS1 active molecules were further divided into training set and test set with the ratio of 70:30. As

PHASE uses only the most active compounds in the training set to create pharmacophore hypothesis, an activity threshold was set for the selection of active ligands ($IC_{50} \leq 1nM$, i.e. $pIC_{50} \geq 9$) and inactive ligands ($pIC_{50} \leq 6.5$) in the training set. The pharmacophore sites were created for all ligand conformers in DS1. These pharmacophore sites are specific chemical features of ligands defined in PHASE as hydrogen bond acceptors (A), hydrogen bond donors (D), hydrophobic groups (H), negatively charged groups (N), positively charged groups (P) and aromatic rings (R).

Target Structure Preparation and Molecular Docking

The X-ray crystal structure coordinates for human ERα ligand-binding domain in complex with 4-hydroxytamoxifen (PDB: 3ERT) was retrieved from the RCSB Protein Data Bank (PDB) and prepared with the Protein Preparation Wizard in MAESTRO v9.2.[19] During the protein preparation, the bond orders were assigned, and hydrogen atoms and formal charges were added to heterogroups. The water molecules within the ligand-binding domain (LBD) were preserved for docking, and all other water molecules 5 Å beyond heterogroups were deleted. The hydrogen bonding network of binding site residues was optimized by selecting the histidine tautomers and by predicting the ionization states. The optimized protein structure was then subjected to all-atom constrained energy minimization using the IMPREF module of MAESTRO v9.2 with OPLS-2005 force field[19]. The prepared ERα structure was used for the molecular docking simulations. The prepared DS1 and DS2 molecule sets were docked flexibly utilizing GLIDE v5.7 standard precision (SP) and GLIDE extra precision (XP) scoring functions.[20] The default settings in the GLIDE were used for both the grid generation and the flexible docking. In addition, molecular docking with PLANTS software was performed using CHEMPLP scoring function with binding site radius 15 Å from the center of the binding cavity, and the results were cluster with RMSD 2.0 Å.[21]

Molecular Dynamics Simulations and Negative-Image Creation

The protein flexibility was introduced in the NIB models by constructing the negative images for an ensemble of protein conformations derived from molecular dynamics (MD) simulation snapshots. For MD, the same protocol was used as previously. [22] In short, the

preparations for MD simulations were performed as follows: (1) The water molecules and the co-crystallized ligand in the crystal structure were removed from ligand binding cavity; (2) Ligand binding cavity was filled with water molecules using VOIDOO/FLOOD[23], (3) TLEAP in ANTECHAMBER 1.27[24] was used for creating force field parameters for the protein (ff03[25]), adding hydrogens and solvating the structure into a 13 Å rectangular box of transferable intermolecular potential three-point water molecules (TIP3P[26]). Then the MD simulations were run with NAMD[27], by using the same parameters that we have successfully employed earlier[22b]. The snapshots at 400 ps intervals were extracted from the MD trajectories with PTRAJ 10 in the ANTECHAMBER 1.27[24] and used for NIB model creation. In principle the NIB models were built as described previously.[10]

Electrostatic Information and Shape Comparison

The electrostatic information of target protein was incorporated into the NIB models through assigning an atom-centered MMFF94 charges[17] for the protein atoms. Then the charges of the protein atoms within 1.8 Å radius of each NIB model data point were averaged and the opposite charge values assigned to the corresponding NIB data point. This particular radius is taken into account due to consideration of atoms within hydrogen bonding distances. The shape comparison and electrostatic matching of the ERα NIB models against the DS1 and DS2 was performed with SHAEP [28], as described in our earlier studies.[10] For electrostatic matching, MMFF94 charges[17] were pre-computed for all molecules in DS1 and DS2.

Fluorescence Polarization and pIC_{50} Values

The pIC50 values of identified molecules were measured using green PolarScreen™ ER Alpha Competitor Assay (Life Technologies, CA, The United States of America) kit. The protocol provided by the manufacturer was followed. Briefly, dilution series where the final concentration of the test compounds ranged between 0.0007 and 10 000 nM was prepared. The test compounds were combined with 25 nM ERα and 4.5 nM fluormone in the assay buffer and placed on black low volume 384-well assay plate with NBS surface (Corning, NY, The United States of America). After mixing the assay plate, it was incubated for 2 hours in

room temperature. The fluorescence polarization was then measured using excitation wave length 485 and emission wave length 535 with bandwidths of 25/20 nm. The measurements were performed on 2104 EnVision® Multilabel Plate Reader which had EnVision Workstation version 1.7 (PerkinElmer, MA, The United States of America).

Synthesis

The coumarin derivatives were synthesized using Perkin-Oglialor condensation reaction. The method was developed from the earlier published procedures and transferred to microwave reactor. [29] The general procedure for the synthesis is shown in Supplementary Fig S1 with detailed synthesis and characterization.

Results and discussion

Validation and Performance Evaluation of Common Pharmacophore Hypothesis Model

The pharmacophore hypotheses were synthesized from six variant lists (A, D, H, N, P, R). The used dataset was divided into training (70%) and test set (30%), where the test set created by PHASE was further verified to contain ligands from all chemotypes and from the most and least active groups. Five combinations of five chemical features were common in all most active ligands (pIC50 ≥ 9), from which the PHASE innate scoring function scores the hypotheses for survival to number of active (pIC50 ≥ 9) and inactive ligands ($pIC_{50} \leq 6.5$). The high ranking hypotheses were used for CPH based 3D-QSAR model building and validation. APRRR-223 (Fig. 1) was identified as the best hypothesis on statistical grounds ($R^2 = 0.923$, standard deviation = 0.317, Fischer significance F = 154.7, and chance correlation P = 4.47×10^{-44}). Survival numbers of active and inactive ligands for the best CPH model were 43.1 and 42.5, respectively. Based on this, it can be said that the DS1-based CPH-based 3D-QSAR model should be highly reliable and thus give accurate predictions.

The selected model, APRRR-223, was mapped on to the most active SERM (ChEMBL198803; 0.2 nM), and the least active SERM (ChEMBL380838; 10,000 nM) in the DS1. While the CHEMBL198803 aligns perfectly with the model, the least active, CHEMBL380838, could not match all the pharmacophore features in the hypothesis, e.g.

CHEMBL380838 does not have an essential chemical feature that matches with positive pharmacophore site. Thus, the derived pharmacophore hypothesis is capable to differentete the most active from the least active SERMs. In total, from the 101 DS1 ligands, the CPH-model identifies 61. However, two active ligands (ChEMBL241301 and ChEMBL391910) in DS1 with $pIC_{50} > 9$ were not mapped into the CPH model and they were consistent outliers for this 3D-QSAR model. The outlying behavior of these ligands is apparent from their very unusual structural features compared to other active ligands in the DS1 data set.

The 3D-QSAR model constructed along with CPH-model has the following statistical parameters: $Q^2 = 0.822$, RMSE = 0.431 and $R^2 = 0.870$. The high Q^2 value shows the accuracy of the model in predicting the ERα activity in the test set. To further evaluate the performance of the 3D-QSAR models, also DS2 was used in the screening process. With compulsory matching of all five pharmacophore features in the hypothesis, out of 39 active ligands and 1395 decoys in the DS2, the hypothesis recognized 16 most active antagonists without selecting any decoys. It must be noted that among the 16 identified DUD antagonists, four already existed in the DS1 and were used in the pharmacophore development and validation. Model was also able to identify chemically distinct antagonists, in contrast to DS1 that belong to the chemotypes of naphthalene, dihydronapthalene, triaryl ethylene and tetracyclic scaffolds. With the objective of recognizing more actives from DS2, the secondary screening was performed with random relaxation of any one of the pharmacophore features from hypothesis (all combinations of four features) that recognized all 39 active ligands and more than 600 decoys (43%). This shows the importance of all five chemical features in APRRR-223 hypothesis (Fig. 1). Accordingly, the hypothesis with all five features is likely to identify most of the highly active ERα ligands, but cannot identify any low-affinity hits in VS campaigns, and if model is relaxed to four features, the disdinguisment of active ligands from inactive molecules becomes highly unreliable.

Molecular Docking

The regression models were derived by correlating the ERα activity and the corresponding docking scores (Fig. 2). The GLIDE SP score based regression model yielded a better correlation coefficient ($R^2 = 0.638$; Fig. 2a) than computationally more demanding GLIDE XP ($R^2 = 0.230$; data not shown). Thus, the GLIDE SP based scoring was used in the model

development and validation. In case of PLANTS docking, the regression model yielded the correlation coefficient R^2 = 0.639 (Fig. 2b) with CHEMPLP score. Accordingly, both GLIDE SP and PLANTS docking produced a very similar and quite reasonable correlation. Furthermore, with the objective of improving the correlation between the ERα activities and docking results, a hybrid regression model was developed of both GLIDE SP score and PLANTS CHEMPLP score. The combination of normalized docking scores of both GLIDE and PLANTS docking resulted better correlation coefficient R^2 = 0.787 (Fig. 2c) than the individual regression models.

The crystal structure of ERα with 4-hydroxytamoxifen reveals the important H-bonding network between Glu353, Arg394, and a water molecule. The visual inspection of the top ranked poses of GLIDE SP and PLANTS CHEMPLP showed a good agreement in binding similarity between the crystal structure ligand and the top-ranked ERα ligands and antagonists. Albeit, GLIDE SP docking poses were observed to have closer resemblance to crystal structure complex conformation than PLANTS docking poses. The docking poses of ligands like ChEMBL81 (Raloxifene), ChEMBL328190 (Lasofoxifene) in DS1 and the most active ERα antagonists in DS2, yielded binding modes that resemble closely the binding mode of 4-hydroxytamoxifen, including similar H-bonding network and hydrophobic contacts. The difference in the docking poses of the most active ligands and the weakly active ligands is that the antiestrogenic side chain (e.g. diethyl amine, pyrrolidine, and piperdine) is able to form an ionic interaction between the amino group of SERMs and carboxylate of Asp351. Note that the ER agonist ChEMBL135 (17β-Estradiol), partial agonists like ChEMBL44 (Genistein), ChEMBL8145 (Daidazin), and ChEMBL30707 (Coumestrol) and other structurally similar ligands in DS1 do not produce ionic interaction with Asp351 due to lack of antiestrogenic side chain.

A summary of receiver operating characteristics (ROC) curves were given as area under curves (AUC) values. The ROC curves plotted for the docking models and for the SHAEP comparisons with NIB models (see below) are shown in Supplementary Fig. S2. The ROC-AUC show better performance for GLIDE SP docking than PLANTS CHEMPLP docking in both DS1 and DS2 (Supplementary Fig. S2). The ROC plot for GLIDE SP with both DS1 and DS2 yielded high AUC = 0.91 ± 0.01 (Table 1). Correspondingly, in case of PLANTS docking model, the ROC plot for DS1 showed AUC = 0.65 ± 0.01 and for DS2 yielded AUC = 0.73 ± 0.01 (Table 1). Overall, the GLIDE SP docking was able to find actives effectively in both DS1

containing larger number of SERMs and in DS2 having lesser volume of antagonists. Even though the AUC for DS2 in PLANTS is higher than for DS1, the early enrichment for DS1 is considerably higher (Table 1, Supplementary Fig. S2). Even if the efficiency of finding the active ligands over decoys with PLANTS CHEMPLP docking model was found slightly lower than with GLIDE SP, PLANTS is still suitable for improving the separation of lower activity molecules from the datasets when used in combination with GLIDE. Therefore, the hybrid docking model was also used for plotting ROC and calculating AUC-values. The ROC plot for DS1 yielded AUC = 0.79 ± 0.01 whereas DS2 gained AUC = 0.86 ± 0.01. The hybrid docking model shows a balanced level of screening performance in separating the active molecules over decoys in both DS1 and DS2.

Selection and Validation Negative Image-Based Models

The X-ray structure analysis of ER-ligand complexes suggests that there are several flexible amino acid residues in the LBDs of ERs, which accordingly means that there is an ensemble of conformations that the LBD can have, depending on the chemical nature of the bound agonist or antagonist. Therefore, the receptor flexibility was introduced in NIB models by using a collection of conformations of the protein derived from MD simulation. Similarly the electrostatic potentials or charge distribution are important in NIB models and depend heavily on the number of water molecules in the LBP and the chemical nature of amino acids lining the LBP.

Initially, a total of 21 NIB models (numbered from 0 to 20; where 0 is the starting structure) were created for LBP of ER at regular intervals from MD simulation. Each of these individual NIB models was screened against DS1 and DS2 using SHAEP. AUC-values for the NIB model search (21 separate models) with DS1 showed AUC ranging from 0.01 to 0.97, whereas with DS2 AUC ranged from 0.38 to 0.85 (data not shown). The highest AUC ≈ 0.97 ± 0.01 with DS1 was obtained for the NIB model 1, i.e. slightly relaxed crystal structure. The above AUC was obtained using the NIB model search with the charge distance of 1.8 Å and the shape and electrostatic weight of 50 %. These parameters for charge distance and electrostatic weighting were chosen based on our previous studies.[10] Correspondingly, NIB model 1 gained AUC ≈ 0.74 ± 0.05 with DS2 in identical search. Furthermore, the binding poses of DS1 ligands on various NIB models were compared with the crystal structure ligand

conformation and their corresponding docking pose. These results suggest that NIB model 1 is the best model in every aspect, and thus, although our initial idea was to use all or at least several NIB models together, as previously,[10b] we decided to use NIB model 1 alone for further evaluation and optimization (Fig. 3).

The selected NIB model 1 was validated by varying the degree of electrostatic weighting from 0 to 100 %, with intervals of 10 % (Table 1). With this procedure we want to control that the electrostatic potentials assigned to the corresponding NIB data points are reasonable and in balance with shape effect i.e. the best electrostatic weighting should be somewhere around 50 %. The shape alone NIB model 1 search resulted an AUC = 0.61 ± 0.03 for DS1. The gradual addition of electrostatic contribution to the NIB model 1 search increased the AUC values from 0.65 ± 0.03 (10 % electrostatic contribution) until 0.97 ± 0.01 and 0.96 ± 0.01 (70 % and 80 % electrostatic contribution, respectively) (Table 1, Supplementary Fig. S3). However, further increase in electrostatic contribution did not improve the AUC values with either of the datasets. The searches with DS1 yielded the poorest AUC-values, when lowest electrostatic contribution was used (shape only to 20 %) (Table 1, Supplementary Fig. S3). These results clearly indicate that the shape alone model is unable to effectively distinguish active molecules over decoys. When considering only the very early enrichment, the top 0.5 % of DS1, the results were almost equally good regardless of the electrostatic contribution, whether with the early enrichment, the top 1 %, the enrichment and number of hits were highest when electrostatic contribution was ≥ 50 % (Table 1). With DS2 the best AUCs were gained when electrostatics was weighted 50 – 70 %, but altogether the results were very even with all comparisons from shape alone up to 70 % electrostatic weighting. Notably, with electrostatic weighting ≥ 90 %, no active molecules were found in the top 10 %.

Because NIB model 1 is not based on the conformer introduced by the crystal structure 3ERT but a slightly relaxed protein structure from the minimizations performed before actual MD simulations, the relaxed protein conformer was also used in docking simulations for reliable comparisons. However, neither GLIDE SP nor PLANTS CHEMPLP benefitted from this. All AUC-values decreased compared to docking with original crystal structure (Table 1). The most notable reduction in AUCs occurred in the GLIDE SP docking with DS1 from 0.91 to 0.73. In fact GLIDE SP was able to dock less active molecules from DS1 when using relaxed protein conformer (only 90 % of the actives). Correspondingly also

absolute enrichments and number of hits decreased (Table 1). Only PLANTS CHEMPLP docking with both DS1 and DS2, showed slender improvement in very early enrichments when relax protein conformer was used.

Identification of ER ligands with VS

Our key attempt was to build a workflow that can be used for reliable prediction of ER binding, and that could be applied, not only in the identification of novel drug candidates, but to predict the environmental toxicity of chemicals, and to enable the prediction of binding for the ligands that are developed for other target proteins in drug discovery, for example 17β-hydroxysteroid dehydrogenase.[6d] Since NIB-model shows excellent AUC-values, the 20 best recognized decoys selected by these models were examined (electrostatic weighting 50 %). Noteworthy, ZINC03826690, identified by 13 NIB-models, was also predicted by the docking to have very high activity (GLIDE SP: -11.43; PLANTS CHEMPLP: -118.8), suggesting a pIC_{50} > 8. Indeed, this compound is a known ERα ligand (pIC_{50}: 8.0), and being thus, inaccurately marked as a decoy in DUD. Furthermore, decoy molecules ZINC02630310 and ZINC03867590 were identified in the top-20 of decoys by several NIB-models, and the docking scores predicted that the pIC_{50}-value for these compounds would be approximately 6.5-7. Unfortunately, these compounds are not commercially available, and thus, cannot be tested. All other decoy molecules were poor based on NIB-models. However, if we consider decoy molecules that are ranked higher than ZINC03826690 by either of the docking methods, we find 12 molecules that all resemble ZINC03826690, indicating that also these molecules could have ER activity (Supplementary, Fig. S4). Unfortunately, these molecules are neither commercially available.

To test the performance of developed models a library of 100,000 drug-like compounds from one commercially available database was screened; unfortunately, we did not identify any potential high affinity molecules (pIC_{50} > 7.0) using combination of four methods: pharmacophore, GLIDE SP, PLANTS CHEMPLP and NIB. This is mainly, because the pharmacophore model with all five features is already too specific for this type of VS campaign, and with four features the model does not discriminate inactives with high enough accuracy (see above). On the other hand, if we only take into consideration both docking methods and NIB-method, five hits remain (Table 2: S1-S5). Only one of these

molecules (S4) showed activity in vitro within concentration range of 0.0007 to 10 000 nM with pIC_{50} value of 6.6. Accordingly, with blind screening where only the numerical comparisons are used, the results contain still lots of inactive ligands.

Next, small virtual library of easy-to-synthesize molecules with 17beta-estradiol sized coumarin-core was screened and analyzed. Again, only docking and NIB-method were able to identify hits. Out of these, few molecules were predicted to be active. Visual inspection revealed that some of the compounds could truly be active ER ligands, and were synthesized. Indeed, when the top five molecules were synthesized and tested *in vitro* they had pIC_{50} values from 5.5 to 6.5 (Table 2: 1-5).

Based on the visual inspection of docking results for identified hit molecules the purchased molecule resembles known partial agonists in size, and the synthesized ligands are similar in size with known agonists. In general, the blind follow of numerical estimations (purchased molecules) yielded molecules that were predicted too optimistically. When prior understanding of known ER-ligands was used in the guidance of molecule design (small virtual library of coumarins), also the activities were predicted more accurately (Fig. 4). In general, the GLIDE SP gave over predictions while PLANTS CHEMPLP under predicted the analyzed molecules.

Conclusions

Here, we have investigated the effectiveness and usefulness of ligand-based method CPH, structure-based methods docking and NIB model as possible VS tools for the identification of novel ERα ligands. This comparison of the above mentioned methods as VS tools describes nicely their different ability to identify active binders for ERα and also helps to better understand the relative advantages and limitations of these methods. The NIB was very efficient in prioritizing the active molecules over a large number of DUD decoys that shows the vitality of the method in structure-based VS for identification novel ERα ligands. The optimized NIB model yields better results for early enrichments than other methods, which is important in VS. Furthermore, the NIB model screening is typically faster to perform than other structure-based methods e.g. docking. Thus, NIB is a feasible option for screening large databases with less computational time and efficiency. The CPH with 3D-QSAR shows that pharmacophore hypothesis finds strictly the most active ligands, but the

prediction capacity is highly chemotype dependent, and in VS campaign done to identify hit molecules, the model has too many features, and if relaxed, too many inactives are identified. The docking (especially GLIDE SP) can be used for the identification of active molecules but above all for improving the estimation of the binding affinities of novel ERα ligands. Accordingly, in a workflow where large compound collection is explored, the initial screening with fast NIB, and then rescoring of the top-ranked hits with accurate docking with careful visual inspection can be recommended.

Acknowledgements

The study was funded by the Academy of Finland (OTP decision number: 250311), the National Doctoral Programme in Nanoscience (SPN). Dr. Risto Juvonen is acknowledged for the help with *in vitro* measurements. CSC, the Finnish IT Center for Science (Espoo, Finland), is gratefully acknowledged for the access to the computational resources (projects: jyy2516 and jyy2585).

References

1. (a) Terstappen, G. C.; Reggiani, A., In silico research in drug discovery. *Trends in pharmacological sciences* **2001,** *22* (1), 23-6; (b) Jorgensen, W. L., The many roles of computation in drug discovery. *Science* **2004,** *303* (5665), 1813-8.

2. Matter, H.; Sotriffer, C., Application and Success Stories in Virtual Screening. In *Virtual Screening - Principles, Challenges, and Practical Guidelines*, 1 ed.; Sotriffer, C., Ed. Wiley-VCH Verlag & Co. KGaA: Weinheim, Germany, 2011; Vol. 49, pp 319-358.

3. Verma, J.; Khedkar, V. M.; Coutinho, E. C., 3D-QSAR in drug design--a review. *Curr Top Med Chem* **2010,** *10* (1), 95-115.

4. Sastry, M.; Lowrie, J. F.; Dixon, S. L.; Sherman, W., Large-scale systematic analysis of 2D fingerprint methods and parameters to improve virtual screening enrichments. *Journal of chemical information and modeling* **2010,** *50* (5), 771-84.

5. (a) Horvath, D., Pharmacophore-based virtual screening. *Methods Mol Biol* **2011,** *672*, 261-98; (b) Leach, A. R.; Gillet, V. J.; Lewis, R. A.; Taylor, R., Three-dimensional pharmacophore methods in drug discovery. *J Med Chem* **2010,** *53* (2), 539-58.

6. (a) Meng, X. Y.; Zhang, H. X.; Mezei, M.; Cui, M., Molecular docking: a powerful approach for structure-based drug discovery. *Current computer-aided drug design* **2011,** *7* (2), 146-57; (b) Koivunen, J. T.; Nissinen, L.; Kapyla, J.; Jokinen, J.; Pihlavisto, M.; Marjamaki, A.; Heino, J.; Huuskonen, J.; Pentikainen, O. T., Fluorescent small molecule probe to modulate and explore alpha2beta1 integrin function. *J Am Chem Soc* **2011,** *133* (37), 14558-61; (c) Koivunen, J. T.; Nissinen, L.; Juhakoski, A.; Pihlavisto, M.; Marjamaki, A.; Huuskonen, J.; Pentikainen, O. T., Blockage of collagen binding to integrin alpha 2 beta 1: structure-activity relationship of protein-protein interaction inhibitors. *Medchemcomm* **2011,** *2* (8), 764-770; (d) Messinger, J.; Hirvela, L.; Husen, B.; Kangas, L.; Koskimies, P.; Pentikainen, O.; Saarenketo, P.; Thole, H., New inhibitors of 17beta-hydroxysteroid dehydrogenase type 1. *Mol Cell Endocrinol* **2006,** *248* (1-2), 192-8.

7. (a) Cross, J. B.; Thompson, D. C.; Rai, B. K.; Baber, J. C.; Fan, K. Y.; Hu, Y.; Humblet, C., Comparison of several molecular docking programs: pose prediction and virtual screening accuracy. *Journal of chemical information and modeling* **2009,** *49* (6), 1455-74; (b) Warren, G. L.; Andrews, C. W.; Capelli, A. M.; Clarke, B.; LaLonde, J.; Lambert, M. H.; Lindvall, M.; Nevins, N.; Semus, S. F.; Senger, S.; Tedesco, G.; Wall, I. D.; Woolven, J. M.; Peishoff, C. E.; Head, M. S., A critical assessment of docking programs and scoring functions. *J Med Chem* **2006,** *49* (20), 5912-31.

8. Scior, T.; Bender, A.; Tresadern, G.; Medina-Franco, J. L.; Martinez-Mayorga, K.; Langer, T.; Cuanalo-Contreras, K.; Agrafiotis, D. K., Recognizing pitfalls in virtual screening: a critical review. *Journal of chemical information and modeling* **2012,** *52* (4), 867-81.

9. (a) Nurminen, E. M.; Pihlavisto, M.; Lazar, L.; Pentikainen, U.; Fulop, F.; Pentikainen, O. T., Novel hydrazine molecules as tools to understand the flexibility of vascular adhesion protein-1 ligand-binding site: toward more selective inhibitors. *J Med Chem* **2011,** *54* (7), 2143-54; (b) Sippl, W., Receptor-based 3D QSAR analysis of estrogen receptor ligands--merging the accuracy of receptor-based alignments with the computational efficiency of ligand-based methods. *Journal of computer-aided molecular design* **2000,** *14* (6), 559-72; (c) Soderholm, A. A.; Lehtovuori, P. T.; Nyronen, T. H., Docking and three-dimensional quantitative structure-activity relationship (3D QSAR) analyses of nonsteroidal progesterone receptor ligands. *Journal of medicinal chemistry* **2006,** *49* (14), 4261-8.

10. (a) Virtanen, S. I.; Pentikainen, O. T., Efficient virtual screening using multiple protein conformations described as negative images of the ligand-binding site. *J Chem Inf Model* **2010,** *50* (6), 1005-11; (b) Niinivehmas, S. P.; Virtanen, S. I.; Lehtonen, J. V.; Postila, P. A.; Pentikainen, O. T., Comparison of virtual high-throughput screening methods for the identification of phosphodiesterase-5 inhibitors. *J Chem Inf Model* **2011,** *51* (6), 1353-63.

11. Shubina, V.; Niinivehmas, S.; Pentikainen, O. T., Reliability of Virtual Screening Methods in Prediction of PDE4Binhibitor Activity. *Curr Drug Discov Technol* **2015,** *12* (2), 117-26.

12. Shang, Y.; Brown, M., Molecular determinants for the tissue specificity of SERMs. *Science* **2002,** *295* (5564), 2465-8.

13. (a) Shen, J.; Tan, C.; Zhang, Y.; Li, X.; Li, W.; Huang, J.; Shen, X.; Tang, Y., Discovery of potent ligands for estrogen receptor beta by structure-based virtual screening. *Journal of medicinal chemistry* **2010,** *53* (14), 5361-5; (b) Knox, A. J.; Meegan, M. J.; Sobolev, V.; Frost, D.; Zisterer, D. M.; Williams, D. C.; Lloyd, D. G., Target specific virtual screening: optimization of an estrogen receptor screening platform. *Journal of medicinal chemistry* **2007,** *50* (22), 5301-10; (c) Therrien, E.; Englebienne, P.; Arrowsmith, A. G.; Mendoza-Sanchez, R.; Corbeil, C. R.; Weill, N.; Campagna-Slater, V.; Moitessier, N., Integrating medicinal chemistry, organic/combinatorial chemistry, and computational chemistry for the discovery of selective estrogen receptor modulators with Forecaster, a novel platform for drug discovery. *Journal of chemical information and modeling* **2012,** *52* (1), 210-24.

14. Gaulton, A.; Bellis, L. J.; Bento, A. P.; Chambers, J.; Davies, M.; Hersey, A.; Light, Y.; McGlinchey, S.; Michalovich, D.; Al-Lazikani, B.; Overington, J. P., ChEMBL: a large-scale bioactivity database for drug discovery. *Nucleic acids research* **2012,** *40* (Database issue), D1100-7.

15. Liu, Y.; Sang, X. T.; Gao, W. S.; Mao, Y. L.; Liu, Y. W.; Liu, H. F.; Yang, Z. Y.; Yang, S. Z.; Zhong, S. X.; Huang, J. F., [The first case of primary epithelial-myoepithelial carcinoma in the liver]. *Zhonghua wai ke za zhi [Chinese journal of surgery]* **2006,** *44* (21), 1477-9.

16. Watts, K. S.; Dalal, P.; Murphy, R. B.; Sherman, W.; Friesner, R. A.; Shelley, J. C., ConfGen: a conformational search method for efficient generation of bioactive conformers. *Journal of chemical information and modeling* **2010,** *50* (4), 534-46.

17. Halgren, T. A., Merck molecular force field. I. Basis, form, scope, parameterization, and performance of MMFF94. *Journal of computational chemistry* **1996,** *17* (5-6), 490-519.

18. Dixon, S. L.; Smondyrev, A. M.; Knoll, E. H.; Rao, S. N.; Shaw, D. E.; Friesner, R. A., PHASE: a new engine for pharmacophore perception, 3D QSAR model development, and 3D database screening: 1. Methodology and preliminary results. *Journal of computer-aided molecular design* **2006,** *20* (10-11), 647-71.

19. Schrödinger Release, Protein preparation wizard, Epik version 2.2, Impact version 5.7, Prime version 3.0, Schrödinger, LLC, New York, NY, 2011.

20. (a) Friesner, R. A.; Banks, J. L.; Murphy, R. B.; Halgren, T. A.; Klicic, J. J.; Mainz, D. T.; Repasky, M. P.; Knoll, E. H.; Shelley, M.; Perry, J. K.; Shaw, D. E.; Francis, P.; Shenkin, P. S., Glide: a new approach for rapid, accurate docking and scoring. 1. Method and assessment of docking accuracy.

Journal of medicinal chemistry **2004,** *47* (7), 1739-49; (b) Friesner, R. A.; Murphy, R. B.; Repasky, M. P.; Frye, L. L.; Greenwood, J. R.; Halgren, T. A.; Sanschagrin, P. C.; Mainz, D. T., Extra precision glide: docking and scoring incorporating a model of hydrophobic enclosure for protein-ligand complexes. *Journal of medicinal chemistry* **2006,** *49* (21), 6177-96.

21. Korb, O.; Stutzle, T.; Exner, T. E., Empirical scoring functions for advanced protein-ligand docking with PLANTS. *J Chem Inf Model* **2009,** *49* (1), 84-96.

22. (a) Postila, P. A.; Ylilauri, M.; Pentikainen, O. T., Full and partial agonism of ionotropic glutamate receptors indicated by molecular dynamics simulations. *J Chem Inf Model* **2011,** *51* (5), 1037-47; (b) Ylilauri, M.; Pentikainen, O. T., Structural mechanism of N-methyl-D-aspartate receptor type 1 partial agonism. *PLoS One* **2012,** *7* (10), e47604; (c) Ylilauri, M.; Pentikainen, O. T., MMGBSA as a tool to understand the binding affinities of filamin-peptide interactions. *J Chem Inf Model* **2013,** *53* (10), 2626-33.

23. Kleywegt, G. J.; Jones, T. A., Detection, delineation, measurement and display of cavities in macromolecular structures. *Acta crystallographica. Section D, Biological crystallography* **1994,** *50* (Pt 2), 178-85.

24. Wang, J.; Wang, W.; Kollman, P. A.; Case, D. A., Automatic atom type and bond type perception in molecular mechanical calculations. *Journal of molecular graphics & modelling* **2006,** *25* (2), 247-60.

25. Duan, Y.; Wu, C.; Chowdhury, S.; Lee, M. C.; Xiong, G.; Zhang, W.; Yang, R.; Cieplak, P.; Luo, R.; Lee, T.; Caldwell, J.; Wang, J.; Kollman, P., A point-charge force field for molecular mechanics simulations of proteins based on condensed-phase quantum mechanical calculations. *J Comput Chem* **2003,** *24* (16), 1999-2012.

26. Aaqvist, J., Ion-water interaction potentials derived from free energy perturbation simulations. *The Journal of Physical Chemistry* **1990,** *94* (21), 8021–8024.

27. Phillips, J. C.; Braun, R.; Wang, W.; Gumbart, J.; Tajkhorshid, E.; Villa, E.; Chipot, C.; Skeel, R. D.; Kale, L.; Schulten, K., Scalable molecular dynamics with NAMD. *J Comput Chem* **2005,** *26* (16), 1781-802.

28. Vainio, M. J.; Puranen, J. S.; Johnson, M. S., ShaEP: molecular overlay based on shape and electrostatic potential. *J Chem Inf Model* **2009,** *49* (2), 492-502.

29. Kirkiacharian, S.; Lormier, A. T.; Resche-Rigon, M.; Bouchoux, F.; Cerede, E., [Synthesis and binding affinity of 3-aryl-7-hydroxycoumarins to human alpha and beta estrogen receptors]. *Ann Pharm Fr* **2003,** *61* (1), 51-6.

Tables and table legends

Table 1. The area under curve (AUC) values, absolute enrichments and number of hits for optimized NIB model 1 with different electrostatics contribution and GLIDE SP, PLANTS CHEMPLP and hybrid docking models with both original crystal structure and relaxed protein conformer

Method	DS1					DS2				
	AUC	Absolute enrichment (amount of hits)				AUC	Absolute enrichment (amount of hits)			
		0.5 %	1 %	5 %	10 %		0.5 %	1 %	5 %	10 %
Protein crystal structure (PDB: 3ERT)										
GLIDE SP	0.91 ± 0.01	12.7 (6)	12.8 (13)	11.5 (58)	7.1 (72)	0.91 ± 0.01	15.8 (3)	13.1 (5)	12.3 (24)	7.5 (29)
PLANTS	0.65 ± 0.01	10.6 (5)	6.9 (7)	8.3 (42)	5.0 (51)	0.73 ± 0.01	10.5 (2)	13.1 (5)	6.6 (13)	3.9 (15)
Hybrid	0.79 ± 0.01	8.5 (4)	6.9 (7)	11.5 (58)	6.2 (63)	0.86 ± 0.01	5.3 (1)	10.5 (4)	9.2 (18)	6.2 (24)
Relaxed protein conformer										
GLIDE SP	0.75 ± 0.01	10.6 (5)	5.9 (6)	5.3 (27)	3.9 (40)	0.89 ± 0.01	5.3 (1)	10.5 (4)	10.7 (21)	7.2 (28)
PLANTS	0.62 ± 0.01	14.8 (7)	7.9 (8)	6.5 (33)	4.5 (46)	0.71 ± 0.01	15.8 (3)	10.5 (4)	5.1 (10)	3.6 (14)
Hybrid	0.73 ± 0.01	10.6 (5)	6.9 (7)	6.5 (33)	4.1 (42)	0.85 ± 0.01	5.3 (1)	10.5 (4)	9.7 (19)	5.7 (22)
SHAEP NIB model 1 (relaxed protein conformer)										
Shape only	0.61 ± 0.03	14.8 (7)	11.9 (12)	4.9 (25)	3.0 (30)	0.72 ± 0.05	15.6 (3)	7.9 (3)	4.6 (9)	3.0 (12)
0 %	0.58 ± 0.03	14.8 (7)	11.9 (12)	4.9 (24)	2.9 (29)	0.72 ± 0.05	15.6 (3)	10.5 (4)	4.6 (9)	3.0 (12)
10 %	0.65 ± 0.03	12.7 (6)	12.8 (13)	4.9 (25)	3.2 (32)	0.72 ± 0.05	15.6 (3)	10.5 (4)	4.6 (9)	3.0 (12)
20 %	0.72 ± 0.02	14.8 (7)	11.9 (12)	4.9 (26)	3.3 (33)	0.73 ± 0.05	15.6 (3)	10.5 (4)	4.6 (9)	3.0 (12)
30 %	0.82 ± 0.02	14.8 (7)	11.9 (12)	5.9 (30)	5.1 (52)	0.73 ± 0.05	21.0 (4)	10.5 (4)	4.6 (9)	3.3 (13)
40 %	0.91 ± 0.02	14.8 (7)	13.8 (14)	10.9 (55)	7.2 (73)	0.73 ± 0.05	21.0 (4)	10.5 (4)	4.6 (9)	3.6 (14)
50 %	0.97 ± 0.02	14.8 (7)	14.8 (15)	14.6 (74)	8.8 (89)	0.74 ± 0.05	21.0 (4)	10.5 (4)	4.6 (9)	3.6 (14)
60 %	0.96 ± 0.01	14.8 (7)	14.8 (15)	14.6 (74)	8.7 (88)	0.75 ± 0.05	21.0 (4)	10.5 (4)	4.6 (9)	3.6 (14)
70 %	0.97 ± 0.01	14.8 (7)	14.8 (15)	14.8 (75)	8.9 (90)	0.74 + 0.05	21.0 (4)	10.5 (4)	5.1 (10)	4.4 (17)
80 %	0.96 ± 0.01	14.8 (7)	14.8 (15)	14.8 (75)	8.8 (89)	0.59 ± 0.05	10.5 (2)	7.9 (3)	4.6 (9)	3.9 (15)
90 %	0.93 ± 0.01	14.8 (7)	14.8 (15)	13.6 (69)	7.9 (80)	0.40 ± 0.04	0.0 (0)	0.0 (0)	0.0 (0)	0.0 (0)
100 %	0.80 ± 0.03	14.8 (7)	14.8 (15)	12.4 (63)	6.5 (66)	0.72 ± 0.05	0.0 (0)	0.0 (0)	0.0 (0)	0.0 (0)

Table 2. The docking scores in GLIDE SP, PLANTS CHEMPLP and normalized GLIDE SP/PLANTS hybrid docking for the purchased (S1-S5) and synthesized (1-5) molecules. From purchased molecules, only S4 showed binding activity when measuring the pIC_{50} values. NB = non binding.

Specs					
Name	**Structure**	**GLIDE SP**	**PLANTS CHEMPLP**	**Hybrid**	**pIC_{50}**
S1	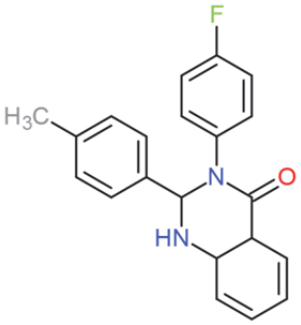	-8.81	-84.67	-8.07	NB
S2	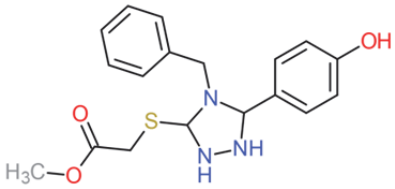	-8.94	-88.37	-8.30	NB
S3	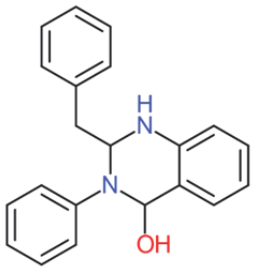	-9.61	-88.85	-8.65	NB
S4	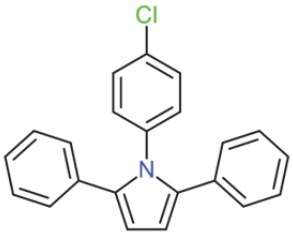	-9.39	-73.80	-7.89	6.6
S5	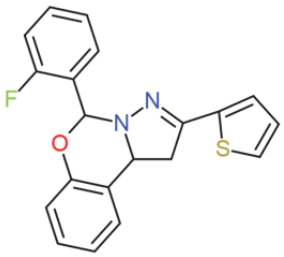	-9.19	-84.73	-8.27	NB

1	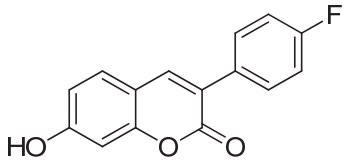	-8.94	-78.05	-7.85	6.1
2	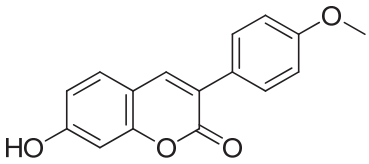	-8.92	-74.07	-7.67	5.9
3	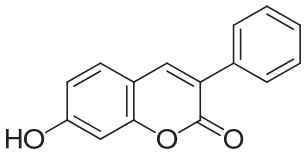	-8.84	-76.04	-7.71	6.5
4	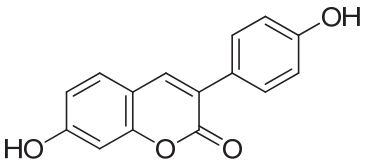	-8.33	-75.24	-7.56	5.5
5	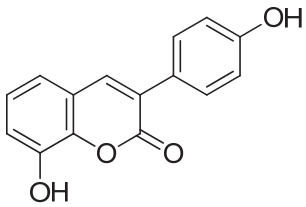	-9.25	-78.32	-7.89	6.5

Figures and figure legends

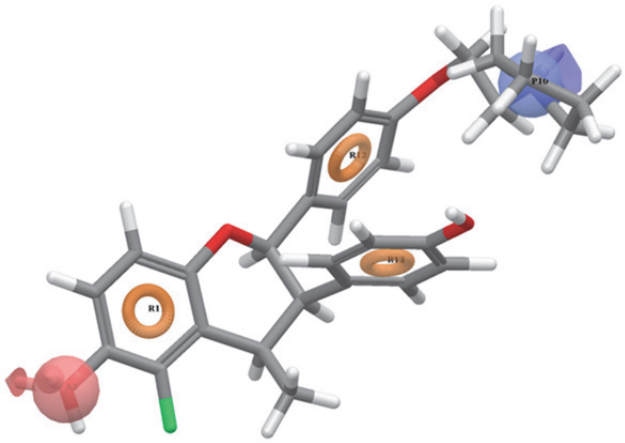

Fig. 1 Common pharmacophore hypothesis (CPH) model showing the essential pharmacophore features for used SERMs. The best CPH model, APRRR-223, represents the pharmacophore features of an ER ligand by way of the reference ligand ChEMBL181369: hydrogen bond acceptor (red spheres with arrows pointing the direction of available lone pairs) and positively charged group at the end of the antagonist-arm (blue sphere with arrow pointing the hydrogen bond direction), and aromatic ring structures in the core of the molecule (orange doughnuts).

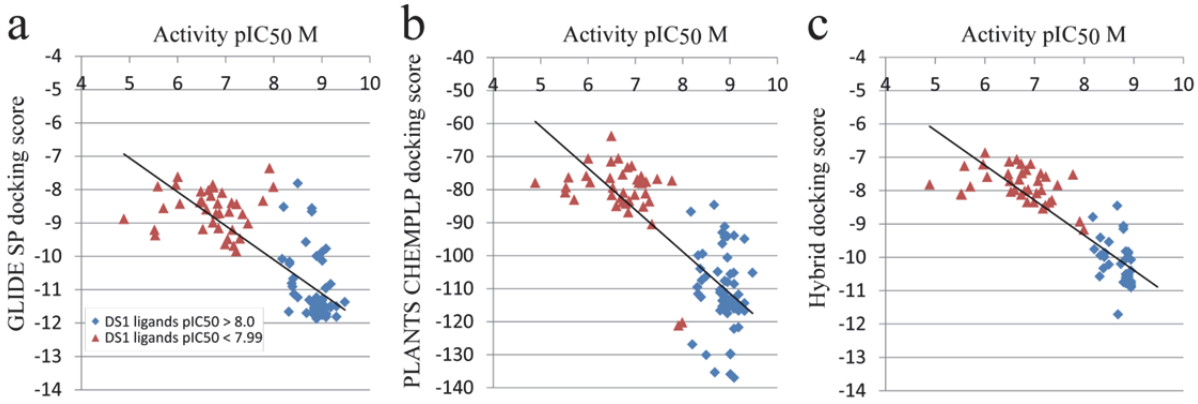

Fig. 2 The predictivity of the docking methods. Correlation of experimental ERα activity of DS1 and DS2 ligands (as pIC_{50}) between (**a**) GLIDE SP, (**b**) PLANTS CHEMPLP, and (**c**) normalized GLIDE SP/PLANTS hybrid docking score are shown.

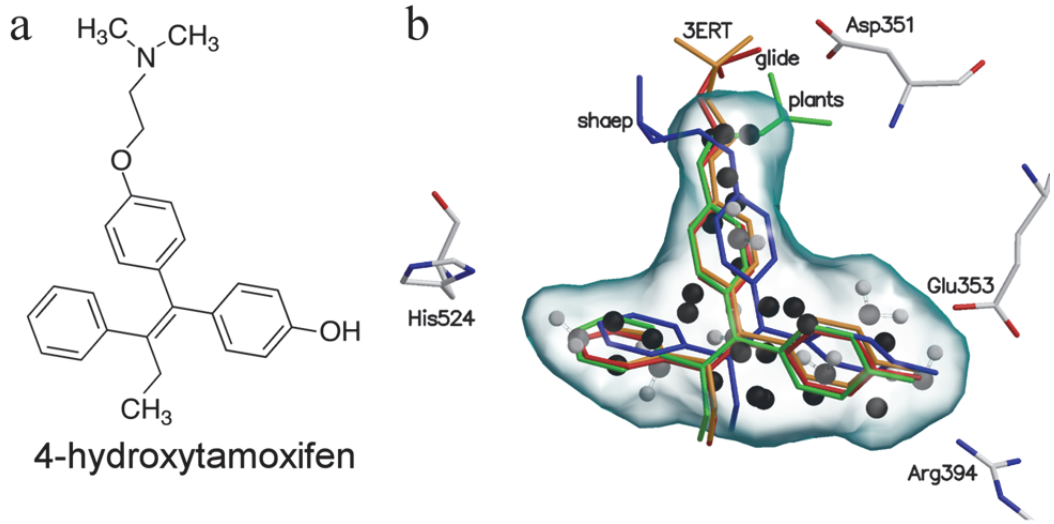

Fig. 3 4-hydroxytamoxifen, the best NIB model along with the key amino acids of the ERα ligand binding pocket with docking results. Figure shows (**a**) the 2D structure of 4-hydroxytamoxifen, and (**b**) its stick model conformations from GLIDE SP (red), PLANTS CHEMPLP (green), and NIB model 1 (blue) superimposed with 3ERT crystal structure ligand (orange). For comparison, panel **b** also shows NIB model 1 as black/white dots, (black dots represent oxygen atoms and white hydrogen atoms of the optimized water molecules, see section *Molecular Dynamics Simulations and Negative-Image Creation*) and pale blue solvent accessible surface. All method are able to produce a representative binding conformation for 4-hydroxytamoxifen.

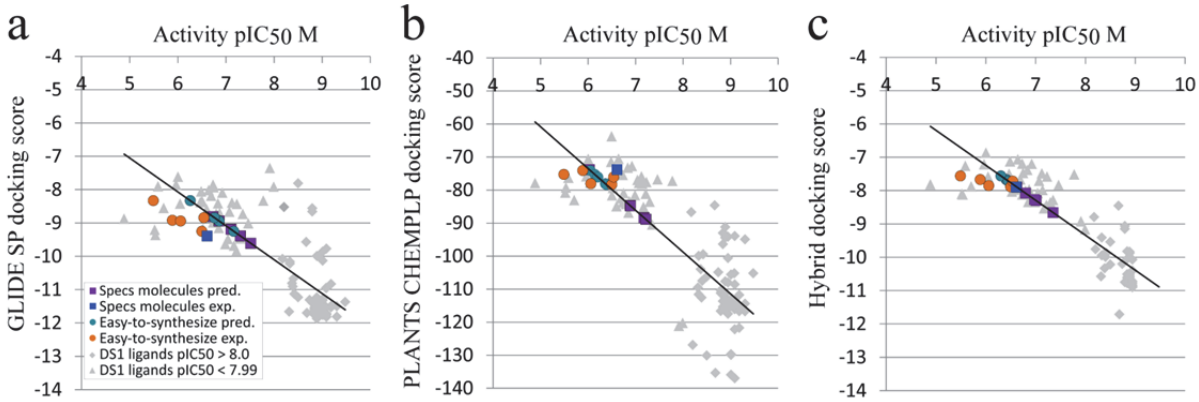

Fig. 4 The correlation of predicted and experimental ERα activity (as pIC_{50}) between docking scores. The predicted and experimental activities are shown for purchased specs molecules and small library of easy-to-synthesize coumarine derivatives as (**a**) GLIDE SP, (**b**) PLANTS CHEMPLP, and (**c**) normalized GLIDE SP/PLANTS hybrid docking scores. The correlation of experimental ERα activity of DS1 and DS2 ligands can be seen on the background.

Electronic Supplementary Information

Supplementary material is listed in the order of appearance in the main text.

Supplementary Table 1. Chemical diversity of DS1 ERα ligands used in this study

Chemotype	n	n %	Activity range pIC_{50}	Activity average
2,3 Diaryl tolylchroman-6-ol	8	7.9	9.1 - 9.5	9.2
2,3 Diaryldihydrobenzoxathin	24	23.8	9.1 - 9.7	9.2
2-Arylbenzo[b]thiophene	3	3.0	8.7 - 9.7	9.2
2-Phenyl spironindene	2	2.0	8.4 - 9.0	8.7
2-Phenyl-1H-indole	9	8.9	8.1 - 9.4	8.8
3,4 Diarylisothiochromanol	5	5.0	9.1 - 9.2	9.1
5,6 diaryl tetrahydronapthol	3	3.0	8.9 - 9.2	9.1
6H-benzo[c]chromene-6-one	8	7.9	5.0 -7.0	6.4
Dihydrobenzoxathin	6	5.9	8.5 - 8.6	8.6
Isoflavone	2	2.0	5.7 - 7.0	6.4
Steroid	5	5.0	5.7 - 8.9	6.8
syn-Dihydrobenzoxathiin	4	4.0	8.6 - 9.3	9.0
Tetrahydrofluorenone-fused pyrazole	9	8.9	6.8 -7.6	7.2
Tetrahydrofluorenone-fused triazole	4	4.0	5.7 - 7.5	6.5
Tetrahydrofluorenone	6	6.0	6.9 - 7.5	7.1
9,10-Dihydrophenanthrene	1	1.0	6.6	6.6
Conformationally restricted tetrahydrofluorenone	1	1.0	7.0	7.0
Coumestan	1	1.0	8.0	8.0

Supplementary Table 2 DS1 ligands and their ERα inhibitory activity data used in this study

S.No	Ligand ID	Chemotype (Subtype or Name)	ERα IC_{50} nM	ERα pIC_{50} M
1	ChEMBL180146	**2,3 Diaryl tolylchroman-6-ol**	0.8	9.1
2	ChEMBL180995	**2,3 Diaryl tolylchroman-6-ol**	0.9	9.0
3	ChEMBL181248	**2,3 Diaryl tolylchroman-6-ol**	0.7	9.2
4	ChEMBL181368	**2,3 Diaryl tolylchroman-6-ol**	0.3	9.5
5	ChEMBL181369	**2,3 Diaryl tolylchroman-6-ol**	0.9	9.0
6	ChEMBL181404	**2,3 Diaryl tolylchroman-6-ol**	0.8	9.1
7	ChEMBL359633	**2,3 Diaryl tolylchroman-6-ol**	0.5	9.3
8	ChEMBL361005	**2,3 Diaryl tolylchroman-6-ol**	0.8	9.1
9	ChEMBL179852	**2,3 Diaryldihydrobenzoxathin**	0.7	9.2
10	ChEMBL182794	**2,3 Diaryldihydrobenzoxathin**	0.7	9.2
11	ChEMBL182980	**2,3 Diaryldihydrobenzoxathin**	0.5	9.3
12	ChEMBL183092	**2,3 Diaryldihydrobenzoxathin**	0.8	9.1
13	ChEMBL183263	**2,3 Diaryldihydrobenzoxathin**	0.5	9.3
14	ChEMBL183333	**2,3 Diaryldihydrobenzoxathin**	0.6	9.2
15	CHEMBL183371	**2,3 Diaryldihydrobenzoxathin**	0.9	9.0
16	ChEMBL183388	**2,3 Diaryldihydrobenzoxathin**	0.9	9.0
17	CHEMBL183467	**2,3 Diaryldihydrobenzoxathin**	0.4	9.4
18	ChEMBL184202	**2,3 Diaryldihydrobenzoxathin**	0.7	9.2
19	ChEMBL184360	**2,3 Diaryldihydrobenzoxathin**	0.6	9.2
20	ChEMBL184367	**2,3 Diaryldihydrobenzoxathin**	0.6	9.2
21	ChEMBL184421	**2,3 Diaryldihydrobenzoxathin**	0.6	9.2
22	ChEMBL184598	**2,3 Diaryldihydrobenzoxathin**	0.8	9.1
23	ChEMBL185083	**2,3 Diaryldihydrobenzoxathin**	0.4	9.4
24	ChEMBL181862	**2,3 Diaryldihydrobenzoxathin**	0.5	9.3
25	ChEMBL361601	**2,3 Diaryldihydrobenzoxathin**	0.4	9.4
26	ChEMBL367350	**2,3 Diaryldihydrobenzoxathin**	0.7	9.2
27	ChEMBL367574	**2,3 Diaryldihydrobenzoxathin**	0.7	9.2
28	ChEMBL368688	**2,3 Diaryldihydrobenzoxathin**	0.9	9.0
29	ChEMBL369545	**2,3 Diaryldihydrobenzoxathin**	0.5	9.3
30	ChEMBL427324	**2,3 Diaryldihydrobenzoxathin**	0.3	9.5
31	ChEMBL433769	**2,3 Diaryldihydrobenzoxathin**	0.3	9.5
32	ChEMBL434525	**2,3 Diaryldihydrobenzoxathin**	0.7	9.2
33	ChEMBL198803	**2-Arylbenzo[b]thiophene**	0.2	9.7
34	ChEMBL372337	**2-Arylbenzo[b]thiophene**	0.6	9.2
35	ChEMBL81	**2-Arylbenzo[b]thiophene (Raloxifene)**	1.8	8.7
36	ChEMBL267385	**2-Phenyl spironindene**	1	9.0
37	ChEMBL281499	**2-Phenyl spironindene**	4.3	8.4
38	ChEMBL46740	**2-Phenyl-1H-indole**	0.6	9.2
39	ChEMBL240438	**2-Phenyl-1H-indole**	2	8.7
40	ChEMBL241256	**2-Phenyl-1H-indole**	6.6	8.2
41	ChEMBL241301	**2-Phenyl-1H-indole**	1	9.0
42	ChEMBL241303	**2-Phenyl-1H-indole**	8	8.1
43	ChEMBL391910	**2-Phenyl-1H-indole**	1	9.0
44	ChEMBL437190	**2-Phenyl-1H-indole**	4	8.4
45	ChEMBL198914	**2-Phenyl-1H-indole (1-Benzyl-sub)**	0.5	9.3
46	ChEMBL372808	**2-Phenyl-1H-indole (1-Benzyl-sub)**	0.4	9.4
47	ChEMBL182690	**3,4 Diarylisothiochromanol**	0.7	9.2

48	ChEMBL182902	**3,4 Diarylisothiochromanol**	0.8	9.1
49	ChEMBL183090	**3,4 Diarylisothiochromanol**	0.8	9.1
50	ChEMBL183399	**3,4 Diarylisothiochromanol**	0.6	9.2
51	ChEMBL304552	**3,4 Diarylisothiochromanol**	0.9	9.0
52	ChEMBL197495	**5,6 diaryl tetrahydronapthol**	0.6	9.2
53	ChEMBL437695	**5,6 diaryl tetrahydronapthol**	0.5	9.3
54	ChEMBL328190	**Tetrahydronaphthalen-2-ol (Lasofoxifene)**	1.3	8.9
55	ChEMBL203072	**6H-benzo[c]chromene-6-one**	129	6.9
56	ChEMBL206500	**6H-benzo[c]chromene-6-one**	229	6.6
57	ChEMBL380717	**6H-benzo[c]chromene-6-one**	716	6.1
58	ChEMBL204922	**6H-benzo[c]chromene-6-one**	159	6.8
59	ChEMBL205934	**6H-benzo[c]chromene-6-one**	785	6.1
60	ChEMBL206547	**6H-benzo[c]chromene-6-one**	101	7.0
61	ChEMBL380838	**6H-benzo[c]chromene-6-one**	10,000	5.0
62	ChEMBL381697	**6H-benzo[c]chromene-6-one**	225	6.6
63	ChEMBL68489	**Dihydrobenzoxathin**	3.1	8.5
64	ChEMBL85090	**Dihydrobenzoxathin**	2.6	8.6
65	ChEMBL85650	**Dihydrobenzoxathin**	3	8.5
66	ChEMBL313941	**Dihydrobenzoxathin**	2.7	8.6
67	ChEMBL315271	**Dihydrobenzoxathin**	3	8.5
68	ChEMBL431611	**Dihydrobenzoxathin**	2.5	8.6
69	ChEMBL8145	**Isoflavone (Daidzein)**	2160	5.7
70	ChEMBL44	**Isoflavone (Genistein)**	92	7.0
71	ChEMBL135	**Steroid (17β)-estra-1,3,5(10)-triene-3,17-diol**	1.35	8.9
72	ChEMBL250110	**Steroid (Androstene-3,5diene)**	110	7.0
73	ChEMBL398456	**Steroid (Androstene-3,5diene)**	1440	5.8
74	ChEMBL77135	**Steroid (Androstenediol)**	210	6.7
75	ChEMBL246138	**Steroid (Androstenediol)**	2240	5.6
76	ChEMBL92660	**syn-Dihydrobenzoxathiin**	2.4	8.6
77	ChEMBL93793	**syn-Dihydrobenzoxathiin**	2	8.7
78	ChEMBL94030	**syn-Dihydrobenzoxathiin**	0.5	9.3
79	ChEMBL94116	**syn-Dihydrobenzoxathiin**	0.51	9.3
80	ChEMBL211349	**Tetrahydrofluorenone-fused pyrazole**	46	7.3
81	ChEMBL211816	**Tetrahydrofluorenone-fused pyrazole**	93	7.0
82	ChEMBL211887	**Tetrahydrofluorenone-fused pyrazole**	82	7.1
83	ChEMBL213829	**Tetrahydrofluorenone-fused pyrazole**	23	7.6
84	ChEMBL215409	**Tetrahydrofluorenone-fused pyrazole**	58	7.2
85	ChEMBL377644	**Tetrahydrofluorenone-fused pyrazole**	176	6.8
86	ChEMBL384268	**Tetrahydrofluorenone-fused pyrazole**	49.2	7.3
87	ChEMBL385680	**Tetrahydrofluorenone-fused pyrazole**	50.9	7.3
88	ChEMBL425439	**Tetrahydrofluorenone-fused pyrazole**	40	7.4
89	ChEMBL214692	**Tetrahydrofluorenone-fused triazole**	34	7.5
90	ChEMBL215802	**Tetrahydrofluorenone-fused triazole**	1906	5.7
91	ChEMBL385949	**Tetrahydrofluorenone-fusedtriazole**	647	6.2
92	ChEMBL441366	**Tetrahydrofluorenone-fusedtriazole**	220	6.7
93	ChEMBL208978	**Tetrahydrofluorenone**	128	6.9
94	ChEMBL209402	**Tetrahydrofluorenone**	30	7.5
95	ChEMBL209429	**Tetrahydrofluorenone**	70.5	7.2
96	ChEMBL209851	**Tetrahydrofluorenone**	141	6.9
97	ChEMBL379821	**Tetrahydrofluorenone**	124	6.9
98	ChEMBL380469	**Tetrahydrofluorenone**	41	7.4
99	ChEMBL205119	**9,10-Dihydrophenanthrene (Effusol)**	240	6.6
100	ChEMBL379008	**Conformationally restricted tetrahydrofluorenone**	97	7.0
101	ChEMBL30707	**Coumestan (Coumestrol)**	11	8.0

Detailed synthesis and characterization data for molecules 1-5.

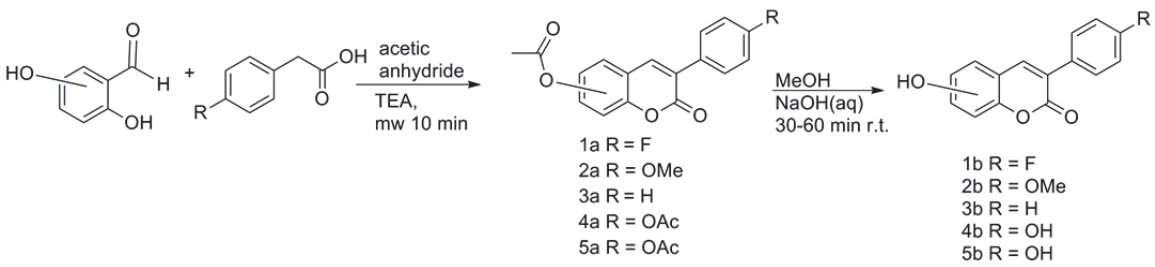

Supplementary Fig. 1. The general procedure for the synthesis of coumarin derivatives

A mixture of salicylaldehyde derivative (2 mmol) and phenyl acetic acid derivative (2.1 mmol), acetic acid anhydride (0.6 ml) and triethylamine (0.36 ml) were placed in a microwave reactor tube and this mixture was heated at 160-170 °C with the CEM Discovery microwave apparatus for 10 min. After cooling, 2 ml of 10% $NaHCO_3$ solution was added and the precipitate was filtered, dried and recrystallized from ETOH/H_2O or acetone/H_2O mixture. The acetyl group(s) were removed by treating the compound with MeOH/NaOH(aq) solution for 30-60 min at r.t.. The solution was acidified with HCl(aq,) and the precipitate was filtered and recrystallized if needed.

Molecule 1

7-acetoxy-3-(4-fluorophenyl)coumarin (1a) [1]

Yield: 92%; m.p. = 204-205 °C (lit. [78] 203-204°C); ^{1}H-NMR (300 MHz, d^6-DMSO) δ: 2.32 (s, 3H, CH_3CO), 7.18 (dd, J^3 = 8.4 Hz, J^4 = 2.1 Hz, 1H, H-6), 7.27-7.33 (m, 3H, H-3' and H-6), 7.75-7.81 (m, 3H, H-2' and H-8), 8.25 (s, 1H, H-4); ^{13}C-NMR (100.6 MHz, d^6-DMSO) δ: 20.82, 109.63, 114.95 (C-3', $J^2_{(C-F)}$ = 21.5 Hz), 115.23 (C-3', $J^2_{(C-F)}$ = 21.5 Hz), 117.26, 118.75, 125.11, 129.41, 130.57 (C-2', $J^3_{(C-F)}$ = 8.3 Hz), 130.68 (C-2', $J^3_{(C-F)}$ = 8.3 Hz), 130.88 (C-1', $J^4_{(C-F)}$ = 3.2 Hz),130.92 (C-1', $J^4_{(C-F)}$ = 3.2 Hz), 140.02, 152.68, 153.38, 159.45, 160.55 (C-4', $J^1_{(C-F)}$ = 245.9 Hz), 163.81 (C-4', $J^1_{(C-F)}$ = 245.9 Hz).

7-hydroxy-3-(4-fluorophenyl)coumarin (1b) [1]

Yield: 81%; m.p. = 237-239 °C (lit. [78] 238-239 °C); ^{1}H-NMR (400 MHz, d^6-DMSO) δ: 6.75 (d, J^4 = 2.3 Hz, 1H, H-8), 6.82 (dd, J^3 = 8.5 Hz, J^4 = 2.3 Hz, 1H, H-6), 7.28 (dd, J^3 = 7.8 Hz, $J^{H,F}$ = 7.8, 2H, H-3'), 7.58 (d, J^3 = 8.5 Hz, 1H, H-5), 7.73 (dd, J^3 = 8.9 Hz, $J^{H,F}$ = 5.5 Hz, 2H, H-2'), 8.14 (s, H-

4), 10.64 (broad) (s, 1H, O-H); ^{13}C-NMR (100.6 MHz, d^6-DMSO) δ: 101.72, 111.90, 113.44, 114.90 (C-3', $J^2_{(C-F)}$ = 22 Hz), 115.12 (C-3', $J^2_{(C-F)}$ = 22 Hz), 121.12, 129.96, 130.32 (C-2', $J^3_{(C-F)}$ = 8 Hz), 130.40 (C-2', $J^3_{(C-F)}$ = 8 Hz), 131.45 (C-1', $J^4_{(C-F)}$ = 3 Hz), 131.48 (C-1', $J^4_{(C-F)}$ = 3 Hz), 141.07, 154.91, 160.07, 160.63 (C-4', $J^1_{(C-F)}$ = 246 Hz), 161.32, 163.07 (C-4', $J^1_{(C-F)}$ = 246 Hz); ESI-MS: *m/z* (rel. abund. %) 279 (M + Na$^+$); elemental anal. for $C_{15}H_9FO_3$, calc. C% 7.31, H% 3.54, found C% 70.16, H% 3.76.

Molecule 2

7-acetoxy-3-(4-methoxyphenyl)coumarin (2a) [1]

Yield: 88%; m.p. = 182-183 °C (lit. [78] 181-182 °C); ^{1}H-NMR (400 MHz, d^6-DMSO) δ: 2.32 (s, 3H, CH_3CO), 3.78 (s, 3H, CH_3O), 7.05 (d, J^3 = 8.9 Hz, 2H, H-3'), 7.17 (dd, J^3 = 8.4 Hz, J^4 = 2.2 Hz, 1H, H-6), 7.29 (d, J^4 = 2.2 Hz, 1H, H-8), 7.70 (d, J^3 = 8.9 Hz, 2H, H-2'), 7.79 (d, J^3 = 8.9 Hz, H-5), 8.19 (s, 1H, H-4); ^{13}C-NMR (100.6 MHz, d^6-DMSO) δ:20.85, 55.22, 109.57, 113.68, 117.49, 118.68, 125.69, 126.72, 129.19, 129.75, 138.62, 152.36, 153.15, 159.59, 168.81; HRMS: *m/z* 333.072 (calc. 333.051) for M + Na$^+$; elemental anal. for $C_{18}H_{14}O_5$, calc. C% 69.67, H% 4.55, found C% 69.58, H% 4.52.

7-hydroxy-3-(4-methoxyphenyl)coumarin (2b) [1]

Yield: 84%; m.p. = 214-215 °C (lit. [78] 215-216 °C); ^{1}H-NMR (400 MHz, d^6-DMSO) δ: , 3.78 (s, 3H, CH_3O), 6.73 (d, J^4 = 2.3 Hz, 1H, H-8), 6.80 (dd, J^3 = 8.5 Hz, J^4 = 2.3 Hz, 1H, H-6), 6.99 (d, J^3 = 8.9 Hz, 2H, H-3'),, 7.55 (d, J^3 = 8.6 Hz, H-5), 7.64 (d, J^3 = 8.9 Hz, 2H, H-2'), 8.07 (s, 1H, H-4), 10.52 (s, 1H, O-H) ;^{13}C-NMR (100.6 MHz, d^6-DMSO) δ: 55.18, 101.66, 112.10, 113.29, 113.61, 121.84, 127.30, 129.48, 129.70, 139.73, 154.64, 159.14, 160.20, 160.88; HRMS: *m/z* 290.969 (calc. 291.063) for M + Na$^+$.

Molecule 3

7-acetoxy-3-phenylcoumarin (3a)

Yield: 90%; m.p. 186-188 °C (lit. [78] 187-188 °C); ^{1}H-NMR as described in literature. [1a]

7-acetoxy-3-phenyl coumarin (3b)

Yield: 90%; m.p. 204-206 °C (lit. [78] 205-206 °C); ^{1}H-NMR as described in literature. [1a]

Molecule 4

7-acetoxy-3-(4-acetoxyphenyl)coumarin (4a) [2]

Yield 89%; %; ^{1}H-NMR (300 MHz, d^{6}-DMSO) δ: 2.30 (s, 1H, CH_3CO), 2.38 (s, 1H, CH_3CO), 7.19 (dd, J^3 = 8.4 Hz, J^4 = 2.2 Hz, 1H, H-6), 7.24 (t, J^3 = 8.7 Hz, 2H, H-3'), 7.31 (d, J^4 = 2.2 Hz, 1H, H-8), 7.77 (t, J^3 = 8.7 Hz, 2H, H-2'), 7.80 (d, J^3 = 8.6 Hz, 2H, H-5), 8.27 (s, 1H, H-4). ^{13}C-NMR (75.48 MHz, d^{6}-DMSO) δ: 20.74, 20.82, 116.97, 119.90, 120.77, 121.67, 125.49, 126.75, 129.74, 131.95, 139.84, 146.44, 150.44, 150.77, 159.51, 169.10, 169.23.

7-hydroxy-3-(4-hydroxyphenyl)coumarin (4b) [3]

Yield 85%; ^{1}H-NMR (300 MHz, d^{6}-DMSO) δ: 6.73 (d, J^4 = 2.2 Hz, 1H, H-8), 6.78-6.84 (m, 3H, H-3', H-6), 7.51-7.57 (m, 3H, H-2´, H-5), 8.01 (s, 1H, H-4), 9.62 (s, 1H, -OH), 10.49 (s, 1H, -OH); ^{13}C-NMR (75.48 MHz, d^{6}-DMSO) δ: 101.64, 112.17, 113.24, 114.98, 122.23, 125.68, 129.49, 129.55, 139.12, 154.52, 157.46, 160.25, 160.71.

Molecule 5

8-acetoxy-3-(4-acetoxyphenyl)coumarin (5a)

Yield 95%; ^{1}H-NMR (300 MHz, d^{6}-DMSO) δ: 2.30 (s, 1H, CH_3CO), 2.40 (s, 1H, CH_3CO), 7.24 (d, J^3 = 8.7 Hz, 2H, H-3'), 7.40 (t, J^3 = 7.8 Hz, 1H, H-6), 7.48 (dd, J^3 = 8.0 Hz, J^4 = 1.7 Hz, 1H, H-7), 7.69 (dd, J^3 = 7.7 Hz, J^4 = 1.7 Hz, 1H, H-5), 7.77 (d, J^3 = 8.7 Hz, 2H, H-2'), 8.32 (s, 1H, H-4); ^{13}C-NMR (75.48 MHz, d^{6}-DMSO) δ: 20.35, 20.83, 120.69, 121.71, 124.55, 125.15, 126.14, 126.53, 129.75, 131.86, 136.75, 140.48, 144.65, 150.80, 158.71, 168.38, 169.12.

8-hydroxy-3-(4-hydroxyphenyl)coumarin (5b) [4]

Yield 85%; m.p. 247-249 °C (lit.[82] 249-250 °C); ^{1}H-NMR (300 MHz, d^{6}-DMSO) δ: 6.84 (d, J^3 = 8.7 Hz, 2H, H-3'), 7.04-7.17 (m, 3H, H-5, H-6, H7), 7.60 (d, J^3 = 8.7 Hz, 2H, H-2'), 8.06 (s, 1H, H-4), 9.70 (s, 1H, -OH), 10.14 (s, 1H, -OH); ^{13}C-NMR (75.48 MHz, d^{6}-DMSO) δ: 115.02, 117.48, 118.31, 120.62, 124.41, 125.29, 126.55, 129.79, 138.89, 141.33, 144.22, 157.91, 159.80.

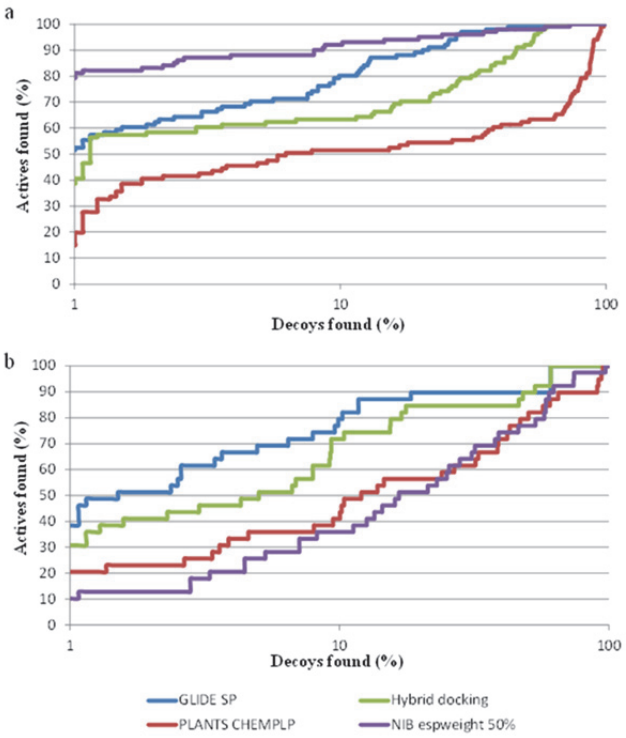

Supplementary Fig. S2 The receiver operating characteristics (ROC) curves of different docking approaches and NIB method on logarithmic scale. ROC curves for GLIDE SP, PLANTS CHEMPLP, hybrid docking models and NIB are shown for both (**a**) DS1 and (**b**) DS2. Figure shows the excellent early enrichments in DS1 (panel **a**), especially with NIB method (purple line).

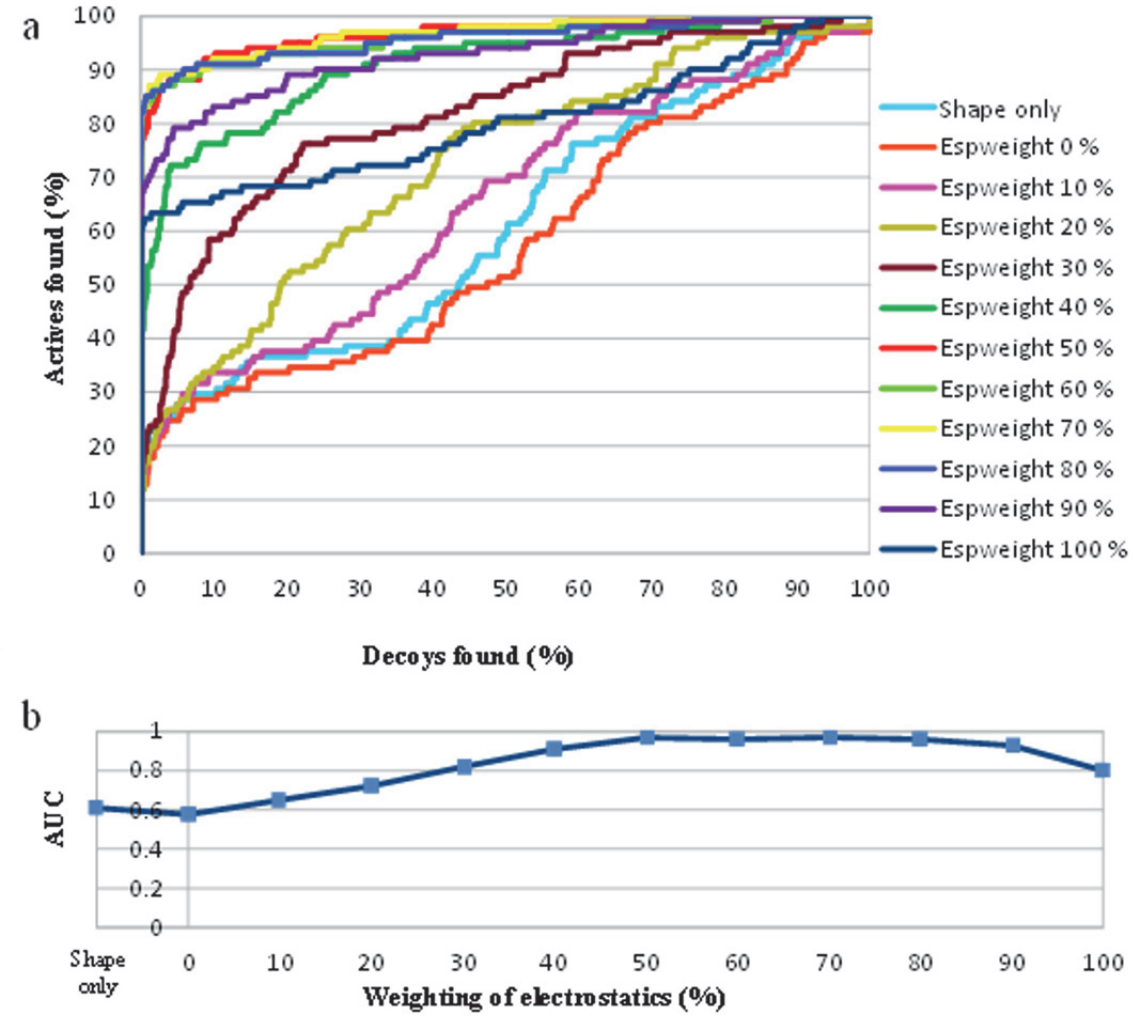

Supplementary Fig. S3 Optimization of the NIB model 1 with varying weighting of electrostatic potentials and shape. ROC curves for NIB model 1 (**a**) show that the best result is achieved using electrostatic weighting of 50 to 80 %. The AUC fluctuates along with the change in electrostatic weighting (**b**) indicating the huge importance of electrostatics in effective distinguishing of active molecules from molecular libraries.

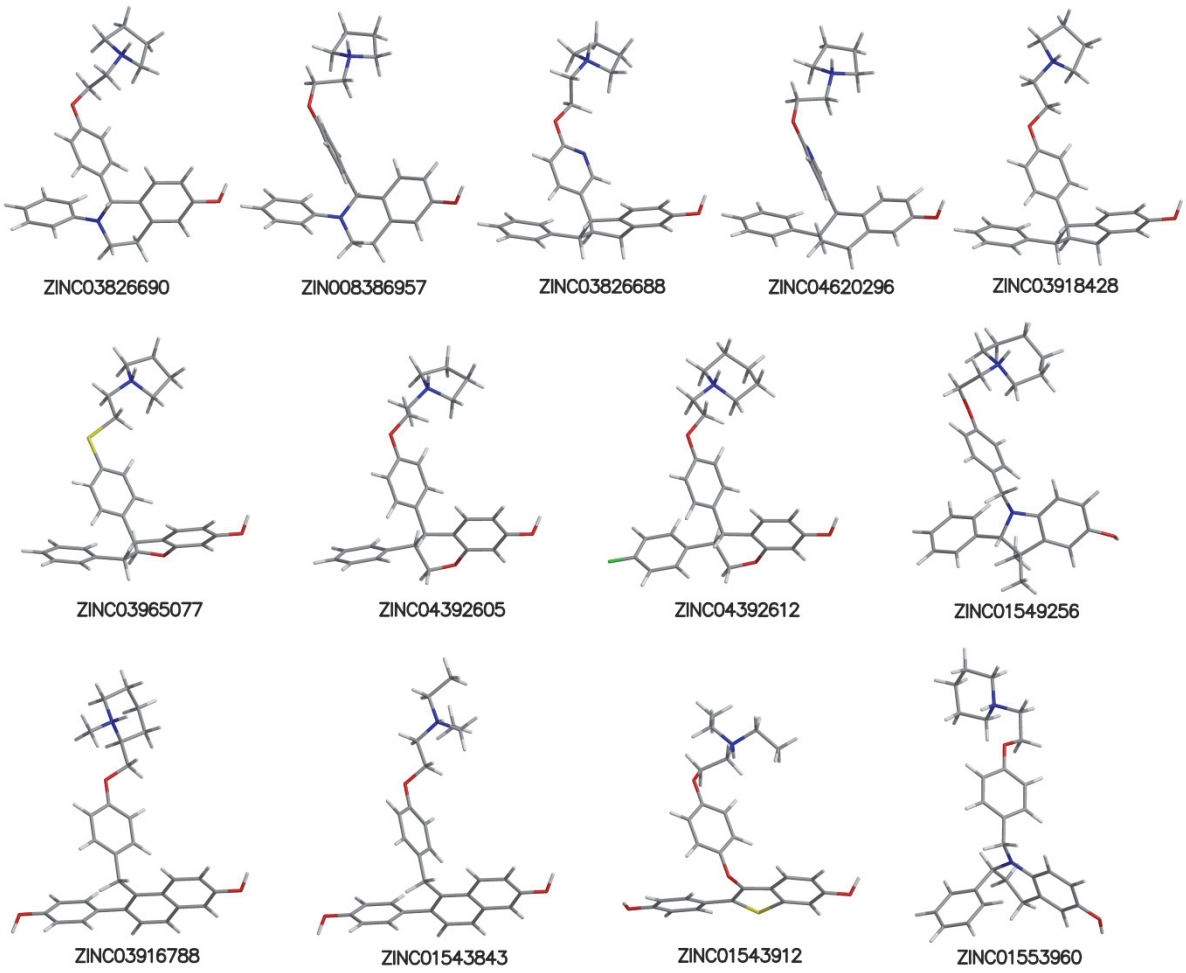

Supplementary Fig. S4 Decoy molecules that are ranked better than ZINC03826690 (really an active molecule) by either GLIDE SP or PLANTS CHEMPLP docking methods.. Twelve molecules resemble active ZINC03826690 considerably, indicating that also these molecules might have ER activity

References

1. (a) Garazd, M. M.; Garazd, Y. L.; Ogorodniichuk, A. S.; Khilya, V. P., Modified coumarins. 29. Synthesis of structural analogs of natural 6-arylfuro[3,2-g]chromen-7-ones. *Chem Nat Compd+* **2009,** *45* (2), 158-163; (b) Kirkiacharian, S.; Lormier, A. T.; Resche-Rigon, M.; Bouchoux, F.; Cerede, E., [Synthesis and binding affinity of 3-aryl-7-hydroxycoumarins to human alpha and beta estrogen receptors]. *Ann Pharm Fr* **2003,** *61* (1), 51-6.

2. Yang, J.; Liu, G. Y.; Dai, F.; Cao, X. Y.; Kang, Y. F.; Hu, L. M.; Tang, J. J.; Li, X. Z.; Li, Y.; Jin, X. L.; Zhou, B., Synthesis and biological evaluation of hydroxylated 3-phenylcoumarins as antioxidants and antiproliferative agents. *Bioorg Med Chem Lett* **2011,** *21* (21), 6420-5.

3. (a) Belluti, F.; Uliassi, E.; Veronesi, G.; Bergamini, C.; Kaiser, M.; Brun, R.; Viola, A.; Fato, R.; Michels, P. A. M.; Krauth-Siegel, R. L.; Cavalli, A.; Bolognesi, M. L., Toward the Development of Dual-Targeted Glyceraldehyde-3-phosphate Dehydrogenase/Trypanothione Reductase Inhibitors against Trypanosoma brucei and Trypanosoma cruzi. *Chemmedchem* **2014,** *9* (2), 371-382; (b) Fais, A.; Corda, M.; Era, B.; Fadda, M. B.; Matos, M. J.; Quezada, E.; Santana, L.; Picciau, C.; Podda, G.; Delogu, G., Tyrosinase Inhibitor Activity of Coumarin-Resveratrol Hybrids. *Molecules* **2009,** *14* (7), 2514-2520.

4. (a) Buuhoi, N. P.; Saintruf, G.; Lobert, B., Oxygen Heterocycles .14. Hydroxylated 3-Aryl- and 3-Pyridyl-Coumarins. *J Chem Soc C* **1969,** (16), 2069-&; (b) Matos, M. J.; Santana, L.; Uriarte, E.; Delogu, G.; Corda, M.; Fadda, M. B.; Era, B.; Fais, A., New halogenated phenylcoumarins as tyrosinase inhibitors. *Bioorg Med Chem Lett* **2011,** *21* (11), 3342-3345.